Biochimica et Biophysica Acta 1808 (2011) 614–621

Contents lists available at ScienceDirect

Biochimica et Biophysica Acta

journal homepage: www.elsevier.com/locate/bbamem

A ToF-SIMS study of the lateral organization of lipids and proteins in pulmonary surfactant systems

Eleonora Keating [a,*], Alan J. Waring [b], Frans J. Walther [c], Fred Possmayer [d,e], Ruud A.W. Veldhuizen [a,f,g], Nils O. Petersen [h]

[a] Lawson Health Research Institute, London, Ontario, Canada
[b] Department of Medicine, UCLA School of Medicine, Los Angeles, Los Angeles Biomedical Research Institute at Harbor-UCLA, Torrance, CA, USA
[c] Los Angeles Biomedical Research Institute at Harbor-UCLA, Torrance, CA, USA
[d] Department of Biochemistry, University of Western Ontario, London, Ontario, Canada
[e] Department of Obstetrics/Gynaecology, University of Western Ontario, London, Ontario, Canada
[f] Department of Physiology and Pharmacology, University of Western Ontario, London, Ontario, Canada
[g] Department of Medicine, University of Western Ontario, London, Ontario, Canada
[h] National Institute for Nanotechnology, Edmonton, Alberta, Canada

ARTICLE INFO

Article history:
Received 9 September 2010
Received in revised form 27 October 2010
Accepted 12 November 2010
Available online 24 November 2010

Keywords:
Pulmonary surfactant
Time-of-flight secondary mass spectrometry
Atomic force microscopy
Lipids proteins lateral organization
Cholesterol
Surfactant function

ABSTRACT

Pulmonary surfactant is a complex lipid–protein mixture whose main function is to reduce the surface tension at the air–liquid interface of alveoli to minimize the work of breathing. The exact mechanism by which surfactant monolayers and multilayers are formed and how they lower surface tension to very low values during lateral compression remains uncertain. We used time-of-flight secondary ion mass spectrometry to study the lateral organization of lipids and peptide in surfactant preparations ranging in complexity. We show that we can successfully determine the location of phospholipids, cholesterol and a peptide in surfactant Langmuir–Blodgett films and we can determine the effect of cholesterol and peptide addition. A thorough understanding of the lateral organization of PS interfacial films will aid in our understanding of the role of each component as well as different lipid–lipid and lipid–protein interactions. This may further our understanding of pulmonary surfactant function.

1. Introduction

Pulmonary surfactant (PS) is a complex mixture of lipids and proteins that is vital for normal breathing. PS is secreted by alveolar type II cells and composed of approximately 80% phospholipids (PLs), 5%–10% neutral lipids (mostly cholesterol) and 5%–10% proteins. The major PL is dipalmitoylphosphatidylcholine (DPPC, 30%–45%). Other major components are unsaturated phosphatidylcholines (PC, 25%–35%) and phosphatidylglycerol (PG) [1]. Four surfactant proteins are present: SP-A, SP-B, SP-C and SP-D which have been found to be important in PS assembly and function [2–4]. SP-A and SP-D are hydrophilic proteins that play a role in transport and storage of PS and in host defense [5]. SP-B and SP-C are hydrophobic proteins that are essential for the biophysical properties of PS such as insertion of phospholipids into monolayers and effective film organization [6]. PS forms a surface active film at the air–water interface of alveoli where it lowers the surface tension. As a result, it prevents alveolar collapse at low lung volumes and lowers the work of breathing [7–9].

Deficiency or dysfunction of PS leads to fatal respiratory disorders such as neonatal respiratory distress syndrome (NRDS) in premature born babies [10] and acute respiratory distress syndrome (ARDS) in children and adults [11]. Clinical surfactant preparations, such as bovine lipid extract surfactant (BLES), are effective in treating NRDS [12] but have proven less effective in treating or ameliorating ARDS [13,14]. Considerable research has been devoted in the past few decades to understand the role of different lipid and protein components of PS. Such investigation should enable us to better understand surfactant function and the changes that occur when PS becomes dysfunctional. This may ultimately aid in preparing more effective therapeutic surfactants.

For many years, surfactant function was explained by the squeeze-out model. It proposed that the fluid non-DPPC components, which are less effective at lowering surface tension, are selectively squeezed out of the film during compression generating a monolayer enriched in the gel phase lipid DPPC at the air–liquid interface of alveoli [8,15,16]. More recent studies provide evidence that a solid, liquid condensed (LC) phase of DPPC is not absolutely necessary to attain

* Corresponding author. Lawson Health Research Institute, 268 Grosvenor St., London, ON, N6A 4V2, Canada.
E-mail address: ekeatin2@uwo.ca (E. Keating).

0005-2736/$ – see front matter © 2010 Elsevier B.V. All rights reserved.
doi:10.1016/j.bbamem.2010.11.015

near zero surface tension at physiological temperatures in vitro [17–20]. Moreover, recent studies using electron microscopy [21,22], atomic force microscopy [23,24], autoradiography [25] and captive bubble tensiometry [22,26] suggest that this surface active film is not composed of a monolayer. Rather, it consists of a surface monolayer plus, in some places, one or more lipid bilayers. These multilayer stacks act as a surface-associated surfactant reservoir that allow surfactant to be re-inserted into the film as surface pressure is lowered on inspiration [26]. Although much effort has been put into understanding how surfactant functions, there is still a lot of uncertainty about the exact mechanism by which surfactant monolayers and multilayers are formed and how they lower surface tension to very low values during lateral compression of PS films.

One technique that may assist in further understanding surfactant function is time-of-flight secondary ion mass spectrometry (ToF-SIMS). This technique can provide information regarding the lateral organization of lipids and peptides in Langmuir–Blodgett (LB) films of natural surfactant and surfactant model systems. Briefly, ToF-SIMS operates by bombarding a sharply focused primary ion beam onto the surface of a sample which induces a collision cascade among the target atoms. This leads to desorption of neutral and ionized species from the surface of the sample. Ionized species are collected and analyzed by a time-of-flight mass spectrometer. In imaging mode, the beam is rastered over the surface of the sample and a full spectrum is collected at each pixel. Thus, a chemical map can be generated showing the lateral distribution of components in a mixture [27].

Based on this information, the objective was to perform proof-of-principle experiments to examine the potential of ToF-SIMS to study the lateral organization of pulmonary surfactant films. To perform these experiments, we studied various surfactant preparations ranging in complexity: from three simple PL mixtures to natural surfactant obtained from the injured lungs of mechanically ventilated rats and from normal lungs obtained from non-ventilated rats. We show that we can successfully image and therefore determine the location of individual PLs, cholesterol and a peptide in interfacial films of these samples. This provides information about phase separation in these systems as well as effect of cholesterol and peptide addition. Also, we show that we can detect changes in lateral organization of PS when it becomes dysfunctional. A thorough understanding of the lateral organization of PS interfacial films will aid in our understanding of the role of each component as well as different lipid–lipid and lipid–protein interactions. This could provide key pieces to the PS function mechanism puzzle as well as have broader implications in more general membrane studies.

2. Materials and methods

2.1. Materials

BLES was a generous gift from the manufacturer (BLES Biochemicals, London, Ontario, Canada) and was extracted before use using a modified Bligh and Dyer technique [28]. Phospholipids and deuterated phospholipids were obtained from Avanti Polar Lipids (Birmingham, AL, USA). Cholesterol was obtained from Sigma (St. Louis, MO, USA) and deuterated-cholesterol was obtained from CDN Isotopes (Pointe Claire, Quebec, Canada). All were received as powders and were dissolved in chloroform at a concentration of 1 mg/mL. miniB is a 34-residue peptide with internal disulfide linkages that is composed of the N- and C-terminal helical regions of SP-B. miniB was isotopically enhanced, synthesized, oxidized-folded and purified as described previously [29]. It has been shown to retain similar activity to full-length SP-B in certain in vitro and in vivo studies [29].

2.2. Rat surfactant isolation

Sprague–Dawley rats (Charles River, St. Constant, PQ, Canada), weighing 350–430 g were acclimatized for a minimum of 3 days with free access to water and standard rodent chow. The ventilation experiments were performed as described previously [30]. Alterations to surfactant precede physiological deterioration during high tidal volume ventilation. Briefly, animals received anesthetic (75 mg/kg Ketamine and 5 mg/kg Xylazine in sterile 0.15 M NaCl) and analgesic (0.05–0.1 mg/kg Buprenorphrine) followed by cannulation of both jugular veins and the right carotid artery. Subsequently, the trachea was exposed and a 14-gauge endotracheal tube was inserted and secured using 2-0 surgical silk. After the tracheotomy, an intravenous injection of a neuromuscular inhibitor (2 mg/kg Pancuronium Bromide) was given to stop spontaneous breathing activity. The animal was immediately connected to a volume-cycled rodent ventilator (Harvard Instruments, St. Laurent, PQ, Canada) and after a stabilization period was ventilated with 100% oxygen using a high tidal volume (high V_t) ventilation strategy ($V_t = 30$ mL/kg, positive-end-expiratory pressure = 0 cm H_2O, at 15–17 breaths per minute). Peak inspiratory pressure was monitored throughout ventilation and arterial blood samples for blood gas measurements were taken at baseline (BL) and every 15 min thereafter.

Following the 2 hours of ventilation, the animals were sacrificed with an overdose of sodium pentobarbital (0.2–0.6 mL 65 mg/mL) administered intravenously to lower blood pressure and exsanguinated via transection of the descending aorta. A midline sternectomy was performed to expose and visualize the lungs. A non-ventilated control group of rats were killed in a similar fashion and used to obtain normal rat surfactant samples. For animals from both groups, a whole lung lavage procedure was performed as previously described [31]. Briefly, 5×10 mL volumes of sterile 0.15 M saline solution were infused and withdrawn from the lungs three times each and the combined lavage volume was centrifuged at 150*g* for 10 min to remove cellular debris. The remaining supernatant was centrifuged at 40,000*g* for 15 min to isolate the pellet containing the large aggregate (LA) subfraction of surfactant which was resuspended in 2 mL of 0.15 M sterile saline and subsequently extracted by the method of Bligh and Dyer. All procedures were approved by the animal use subcommittee at the University of Western Ontario, under the guidelines of the Canadian Council of Animal Care.

2.3. Langmuir–Blodgett (LB) film preparation

A Kibron μTrough SE (Helsinki, Finland) was used to prepare the LB films. The Langmuir balance is equipped with a continuous teflon ribbon to minimize film leakage. The trough contains ~90 mL subphase and has a working area of ~125 cm^2. All samples were dissolved in chloroform and were spread drop-wise on room-temperature Millipore purified water. At least 10 min was allowed before compression for the solvent to evaporate and for the film to equilibrate. The films were then compressed at a rate of 0.02 $nm^2\ molecule^{-1}\ min^{-1}$ in constant pressure mode to the desired surface pressure of 30 mN/m. Monolayer films were deposited onto substrates by elevating the previously submerged substrates vertically through the air–water interface at a rate of 2.0 mm/min. Gold-coated mica was used as the substrate in all experiments. Gold-coating was achieved by inserting freshly cleaved 1×1 cm^2 pieces of mica into a Hummer VI sputtering system (Technics EM, Springfield, VA) under reduced pressure at 100 mTorr. The Au was sputtered onto the substrate for 10 min at a plate current of 10 mA. Deposited films were imaged within 2 hours of deposition.

2.4. Time-of-flight secondary ion mass spectrometry (ToF-SIMS) imaging

ToF-SIMS images were collected using an ION-TOF ToF-SIMS IV (ION-TOF, Munster, Germany) equipped with a bismuth liquid ion

source at ACSES, University of Alberta, and Surface Science Western, University of Western Ontario. The primary analysis beam was 25 keV Bi^{3+} operated in burst alignment mode with 10 kHz repetition rate and a pulse width of 100 ns. The target current was <0.2 pA and the spot size was estimated to be ~300 nm. Mass analysis was performed via a single stage reflectron ToF analyzer at 2 keV with 10 keV post acceleration. The mass range was 0–800 amu with unit mass resolution. Negative secondary ion images were acquired from regions of interest, typically with a $50\times50\ \mu m^2$ primary beam raster size. A 256×256 pixel image resolution was chosen, given the beam spot size and the raster area used in this work. The negative secondary ion images of interest were reconstructed from the raw data stream. Each image is normalized in intensity according to the minimum and maximum counts in a single pixel; these values are then mapped to a 256 increment, thermal color scale. The thermal gradient is chosen such that brighter areas in an image correspond to areas of increased secondary ion yield. In some cases, the ToF-SIMS images were processed to enhance contrast by using a smoothing function available as part of the ION-TOF software.

2.5. Atomic force microscopy imaging

Topographical atomic force microscope (AFM) images were obtained using a Nanoscope III scanning force multimode microscope (Digital Instruments, Santa Barbara, CA). Samples were scanned in contact mode in air within 2 hours of deposition. A silicon nitride cantilever was used with a spring constant of 0.3 N/m and the scanner was of the J type. Image analysis was performed using the Nanoscope III software (version 5.12r3).

3. Results

3.1. Chemical imaging of a lipid mixture

In order to understand the properties of surfactant, studies have been conducted utilizing mixtures of three of the most abundant PLs present in pulmonary surfactant, DPPC, POPC and POPG. The phase behavior of these types of mixture is well established, where lateral pressure leads such monolayers to form “domains” where unsaturated PLs are generally present in the liquid expanded phase (LE) and the saturated PLs are concentrated in the LC phase. This first experiment used these established properties of such a mixture to test the ability of ToF-SIMS to determine the lateral distribution of these PLs in an LB film. In order to accomplish this, ions specific to each component must be selected. These could be fragment ions or secondary ions of the intact species. The ionization yield is low at the higher masses and therefore, the contrast in the images of the molecular ions tends to be poorer. In addition, these 3 PLs are chemically very similar and will therefore fragment in a similar fashion. For example, all species share the palmitic acid unit, two PLs share the phosphatidylcholine unit and two share the oleic acid unit. To resolve this difficulty, deuterated analogues are commonly used in ToF-SIMS experiments. It has been shown that the incorporation of deuterium into the lipid chains does not alter the miscibility or phase behaviour of these systems [32] and also these deuterated analogues have the same fragmentation pattern within a ToF-SIMS experiment [33]. Therefore, fragment ions from deuterated analogues should easily be distinguished from those arising from the isotopically unlabelled lipids by the difference in masses.

Figs. 1A–C show representative ToF-SIMS images collected in positive ion mode for an LB sample of 50:30:20 d4-DPPC:POPC:d31-POPG compressed and deposited at a surface pressure of 30 mN/m. The deuterium is located in the head group of DPPC and the acyl chain of POPG. Under bombardment, these 3 PLs generate a large number of ions from the head group and acyl chains; however, we successfully chose 3 ions which unambiguously give the lateral distribution of each component. Figs. 1A–C correspond to M50 ($C_3D_7^+$) which is a deuterated fragment from the acyl chain of d31-POPG, M184 ($C_5H_{15}NPO_4^+$) derived from the head group of POPC and M188 ($C_5H_{11}D_4NPO_4^+$) specific to d4-DPPC, respectively. At this surface pressure, phase separated domains form in the monolayer which range in diameter from 2 to 10 μm. These data correlate well with the known behaviour of this lipid mixture, with the unsaturated PLs (POPC and d31-POPG) present mainly in the liquid expanded phase (LE), and the saturated PL (d4-DPPC) concentrated in the LC phase.

Atomic force microscopy (AFM) was also used to confirm domain formation. Fig. 1D shows a topographical image of a 50:30:20 d4-DPPC:POPC:d31-POPG compressed to a surface pressure of 30 mN/m and transferred onto mica by Langmuir–Blodgett technique. For AFM imaging, we did not use gold-coated mica, which is the substrate used in ToF-SIMS experiments because of interference from reflection. This image shows that two types of LC domains form LC micro-domains which have an average diameter of ~5 μm, similar to the domains seen in the ToF-SIMS images in Figs. 1A–C and nano-domains with an average diameter of ~100 nm. A zoomed-in AFM image is inserted in Fig. 1D to clearly show the presence of nano-domains. We have performed extensive height analysis of nano and micro-domains (data not shown) and we found their height difference to be similar at ~0.9 nm. Since their height analysis is similar, we conclude that their lipid composition is likely similar. LC nano-domains are not resolved by ToF-SIMS due to their size; however, they may explain the presence of DPPC outside LC domains seen in Fig. 1C.

Lipid mixtures can be altered further to, for example, determine the lateral distribution of cholesterol. In the second lipid mixture experiment, we added 30 mol% of a deuterated analogue of cholesterol (d7-cholesterol) to a PL mix of 50:30:20 DPPC:POPC:POPG. Although 30 mol% is relatively high compared to previous

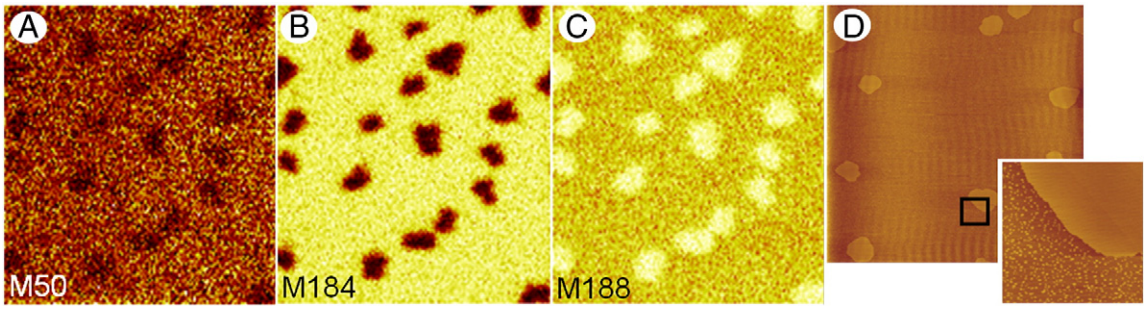

Fig. 1. ToF-SIMS (A–C) and AFM (D) images of a 50:30:20 d4-DPPC:POPC:d31-POPG film compressed to a surface pressure of 30 mN/m and transferred onto gold-coated mica (A–C) and freshly cleaved mica (D) by conventional Langmuir–Blodgett deposition. Maps of positive SI showing fragment ions M50 (A), M184 (B) and M188 (C) specific to d31-POPG, POPC and d4-DPPC, respectively. All ToF-SIMS images are $50\times50\ \mu m^2$, 256×256 pixels with 1 shot/pixel. AFM image is $60\times60\ \mu m^2$ and the high magnification AFM image inserted shows a zoomed-in view of the area indicated by the black box.

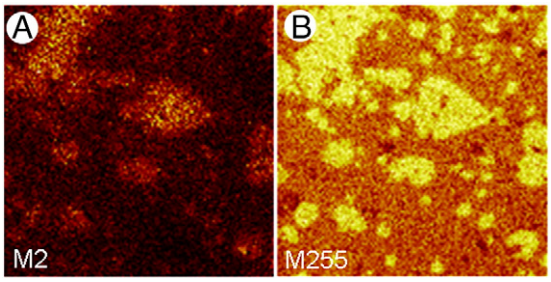

Fig. 2. ToF-SIMS images of 50:30:20 DPPC:POPC:POPG supplemented with 30 mol% d7-cholesterol film compressed to a surface pressure of 30 mN/m and transferred onto gold-coated mica by conventional Langmuir–Blodgett deposition. Maps of negative SI showing M2 (A) which corresponds to deuterium and gives the location of d7-cholesterol and M255 (B) which corresponds to palmitate. Both images are $100 \times 100\ \mu m^2$, 256×256 pixels with 1 shot/pixel.

studies, it was required to ensure an appropriate SI yield to obtain sufficient contrast in ToF-SIMS images. Representative negative ion mode images of an LB film compressed to 30 mN/m are shown in Figs. 2A and B. The image of palmitic acid (Fig. 2B) reveals the presence of domains under these conditions. Fig. 2A shows the distribution of deuterium and therefore the location of cholesterol within domains as would be expected considering that the hydroxylic group of cholesterol interacts preferentially with the head groups of DPPC and DPPG [34].

3.2. Chemical imaging of an exogenous therapeutic surfactant—bovine lipid extract surfactant (BLES)

Whereas imaging simple lipid mixtures, as described above, is fairly straightforward especially when using deuterium analogues, naturally derived exogenous surfactant preparations, such as bovine lipid extract surfactant (BLES), are compositionally more complex and are less well characterized in terms of phase separation. BLES is a clinical surfactant used to treat neonatal respiratory distress syndrome (NRDS) developed by premature babies who do not have sufficient amounts of surfactant. Compositionally, BLES is well characterized and consists of two surfactant associated proteins, SP-B and SP-C, a low amount of cholesterol and a complex PL profile that includes DPPC, various other PC species, both disaturated and unsaturated PG molecules as well as minor levels of other phospholipids. Elucidating the lateral distribution of these various components in BLES would enhance our understanding of how specific components interact and possibly lead to a better understanding of surfactant function mechanism. As mentioned in the previous section, multiple components of pulmonary surfactant may fragment in a similar fashion which makes the selection of specific ion fragments very difficult. Although BLES cannot be made up of solely deuterium labeled lipids, samples can be modified by adding cholesterol or spiked with small amounts of specific deuterated PLs or ^{15}N-labeled peptide, in order to enhance the detection of those molecules.

To localize specific phospholipids in BLES, our third experiment utilized BLES samples spiked with various lipids; the first sample was labeled with 10 mol% d4-DPPC, the second with 5 mol% d31-POPC and the third with 5 mol% d31-POPG. Figs. 3A–C show representative ToF-SIMS images collected in negative ion mode. Each image shows the lateral distribution of M2. All contributions to M2 in negative ion mode are due to deuterium; therefore, these images show the lateral distribution of d4-DPPC, d31-POPC and d31-POPG, respectively, in the three different samples. The SI yield of M2 was low which can be seen as low intensity. To improve the contrast and therefore better visualize the location of PLs, the images were subjected to a smoothing function available as a part of the ToF-SIMS software. The resulting images, shown in Figs. 3A1–C1, show domain formation due to phase separation with diameters ranging from 8 to 15 μm. The d4-DPPC is concentrated in solid LC domains, while d31-POPC is present in the fluid LE phase. Interestingly, d31-POPG is mainly present in the LE phase but in some cases shows an increased concentration around the edges of LC domains.

In addition to lipids, BLES also contains hydrophobic proteins SP-B and SP-C. Under bombardment by the primary beam of a ToF-SIMS instrument, proteins have a characteristic fragmentation pattern characteristic of the amino acid composition. Other ToF-SIMS studies using reconstituted surfactant systems have deciphered typical SI fragments corresponding to surfactant-associated proteins; however, in more complex systems, such as a natural pulmonary surfactant, signals arising from various lipids and proteins often show significant interference making it difficult to determine their location. To avoid this difficulty, we added a ^{15}N-labeled peptide (miniB) to BLES and determined its lateral distribution in an LB film. miniB is a 34-residue

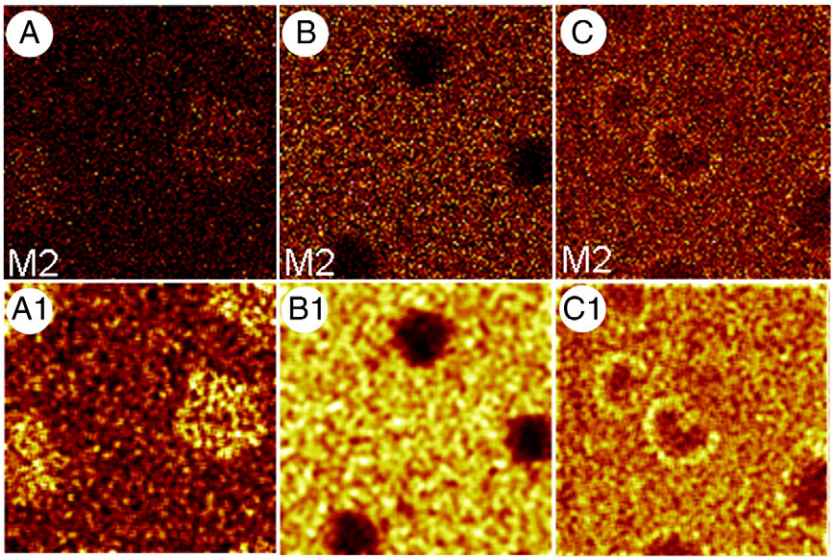

Fig. 3. ToF-SIMS negative ion mode images of M2 (deuterium) for 3 LB films: BLES + 10 mol% d4-DPPC (A), BLES + 10 mol% d31-POPC (B) and BLES + 10 mol% d31-POPG (C) compressed and deposited at a surface pressure of 30 mN/m. Images A1–C1 were obtained by subjecting A–C to a smoothing function available as part of the ION-TOF software to increase contrast. All images are $50 \times 50\ \mu m^2$, 256×256 pixels with 1 shot/pixel.

peptide with internal disulfide linkages that is composed of the N- and C-terminal helical regions of SP-B. It has been shown to retain similar activity to full-length SP-B in certain in vitro and in vivo studies [29]. Therefore, we expect miniB to be found in the same location as SP-B.

M45, corresponding to $C_2H_6^{15}N^+$, was selected to unambiguously determine the lateral distribution of miniB in a BLES LB film compressed to a surface pressure of 30 mN/m. Figs. 4A–D are ToF-SIMS images collected in positive and negative ion modes and correspond to $C_2H_6^{15}N^+$ (M45) from miniB, palmitic acid (M255), $DPPG^-$ molecular ion (M722) and $POPG^-$ parent ion (M747), respectively. Because the SI yield of some of these ions was low, all images were subjected to a smoothing function to improve contrast and therefore, more clearly show the lateral distribution. The palmitic acid image clearly reveals the presence of domains with diameter in the range of 2–8 μm. The saturated PL, DPPG, is concentrated within these domains while the unsaturated PL, POPG, is present outside domains. These results indicate that domain formation is due to phase separation. Fig. 4A1 shows that the peptide, miniB, is associated with the fluid, LE phase.

In addition to determining the localization of specific components within the surface film, ToF-SIMS can also be utilized to examine whether the distribution of one component is affected by the presence of another. For example, it has been proposed that cholesterol can modulate structural organization of a surface film. Our lab has shown that addition of physiological amounts of cholesterol to BLES leads to the formation of domains within liquid condensed domains at low surface pressure as well as an increase in the number of liquid condensed domains and a decrease in their average diameter. The experiments performed for Figs. 5 and 6 address this phenomenon by examining the lateral distribution of PLs or of miniB after supplementing BLES with cholesterol. 20 mol% cholesterol was added to BLES in the experiment for Fig. 5. Fig. 5A corresponds to M735 which shows the distribution of the DPPC-H^+ molecular ion and Fig. 5B corresponds to M722 showing the distribution of $DPPG^-$ molecular ion. These images unambiguously show that DPPC and DPPG are still concentrated within domains. Furthermore, DPPG seems to be heterogeneously distributed within domains, separating perhaps within the third phase, Lo, induced by the presence of cholesterol as suggested by previous studies.

To examine whether the distribution of miniB is affected by the presence of cholesterol, we added 30 mol% d7-cholesterol to BLES in the presence of 20 mol% ^{15}N-miniB. ToF-SIMS images of such an LB film compressed to a surface pressure of 30 mN/m are shown in Fig. 6. All images shown in Figs. 6 (A–E) were subjected to a smoothing function to improve contrast and the resulting images are labeled as A1–E1, respectively. The palmitic acid image (M255) shows the formation of domains. Molecular ion images for $DPPG^-$ and $POPG^-$ show that the saturated PL is present within domains while the unsaturated PL is present outside domains. These results also indicate that phase separation occurs under these conditions. Based on the distribution of deuterium, we conclude that cholesterol is concentrated inside domains. It is known that in the presence of cholesterol, Lo and LC phases exist and are seen as domains within condensed domains. Unfortunately, due to low SI yield, it is difficult to conclude whether the distributions of DPPG and cholesterol are heterogeneous. M45 ($C_2H_6^{15}N^+$) was selected to show the location of miniB in the fluid, LE phase. This indicates that the distribution of the peptide is not affected by the presence of cholesterol.

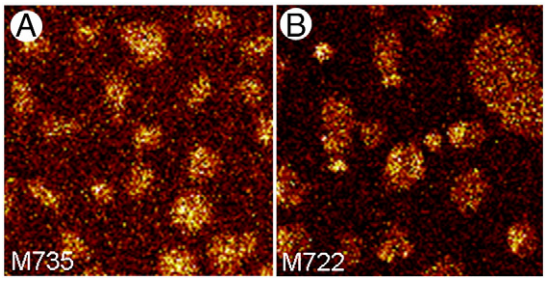

Fig. 5. ToF-SIMS images showing the effect of cholesterol on the lateral organization of DPPC and DPPG in BLES LB films. BLES was supplemented with 20 mol% cholesterol and a film was compressed to a surface pressure of 30 mN/m and transferred onto gold-coated mica by conventional Langmuir–Blodgett technique. Image A was collected in positive ion mode and shows the distribution of M735 (DPPC-H^+) and image B was collected in negative ion mode and shows the distribution of M722 ($DPPG^-$). Both images are 50×50 μm^2, 256×256 pixels with 1 shot/pixel.

3.3. Chemical imaging of PLs in rat pulmonary surfactant

The final experiment focused on utilizing ToF-SIMS for imaging a natural surfactant. Lateral distribution of surfactant components within the films of natural surfactant would not only provide insight

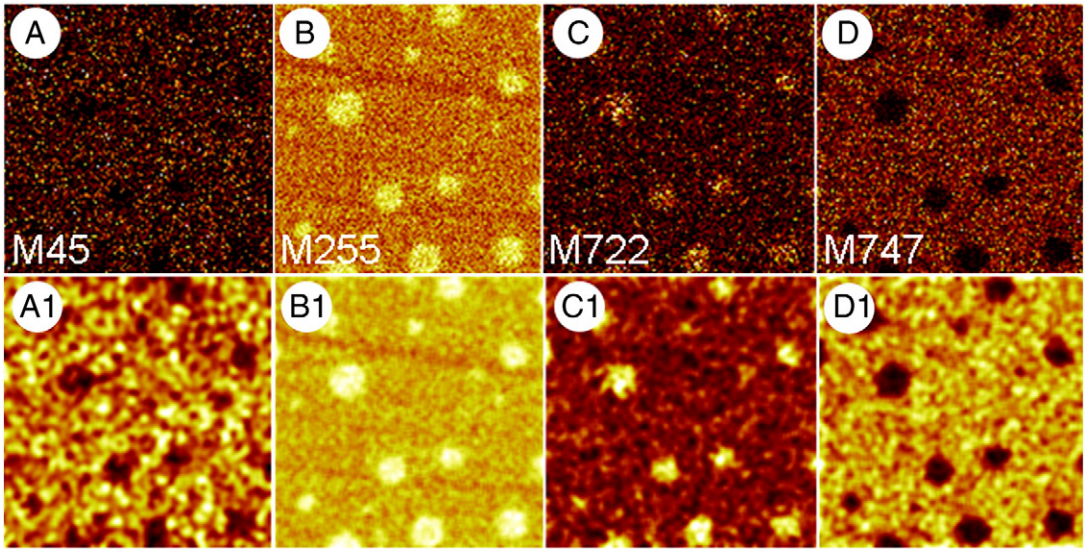

Fig. 4. ToF-SIMS images of a BLES LB film supplemented with 20 mol% ^{15}N-miniB compressed to a surface pressure of 30 mN/m and transferred onto gold-coated mica by conventional Langmuir–Blodgett technique. A–D are SI maps showing the distribution of M45 ($C_2H_6^{15}N^+$) specific to ^{15}N-miniB, M255 (palmitate), M722 ($DPPG^-$) and M747 ($POPG^-$). Images shown in A1–D1 were obtained by subjecting A–D to a smoothing function available as part of the ION-TOF software to increase contrast. All images are 50×50 μm^2, 256×256 pixels with 1 shot/pixel.

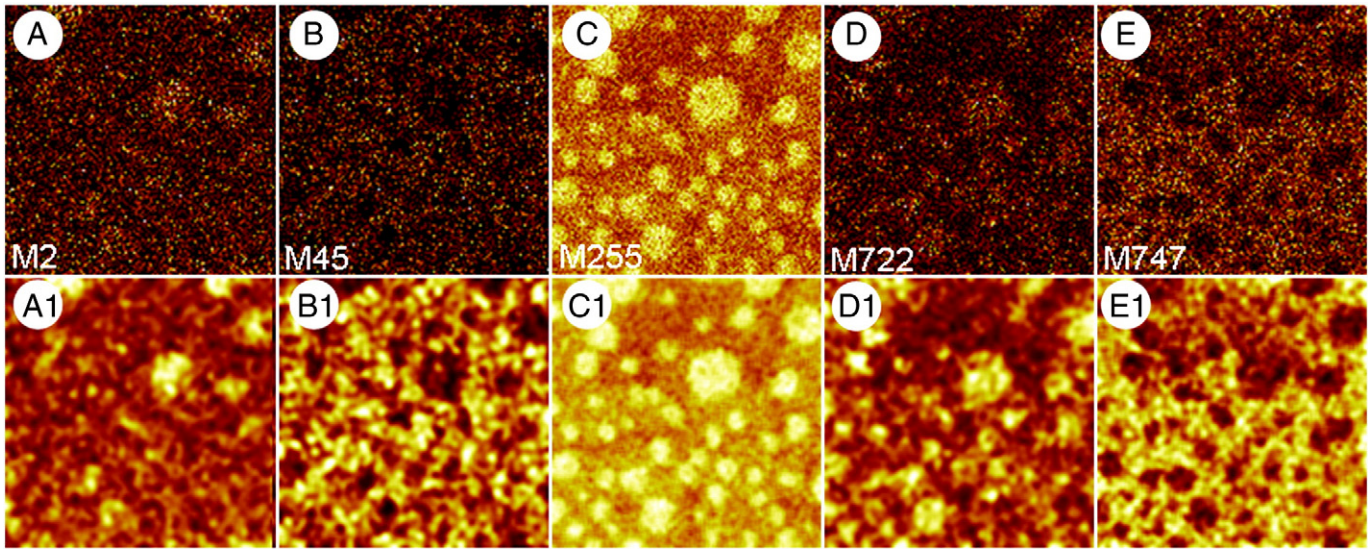

Fig. 6. ToF-SIMS images showing the effect of cholesterol on the lateral distribution of miniB and PLs in BLES LB films. BLES supplemented with 20 mol% ^{15}N-miniB and 20 mol% d7-cholesterol was compressed to a surface pressure of 30 mN/m and transferred onto gold-coated mica by conventional Langmuir–Blodgett technique. A–E were collected in positive and negative ion modes and show the distribution of M2 (deuterium) specific to d7-cholesterol, M45 ($C_2H_6^{15}N^+$) specific to ^{15}N-miniB, M255 (palmitate), M722 ($DPPG^-$) and M747 ($POPG^-$), respectively. A1–E1 were obtained by subjecting A–E to a smoothing function available as part of the ION-TOF software to improve contrast. All images are 50×50 μm^2, 256×256 pixels with 1 shot/pixel.

into its function but it could also be utilized to study dysfunction and correlate with physiological studies. In the current experiment, we used natural surfactant which was lavaged from the lungs of rats which were injured by mechanical ventilation with high tidal volume V_t and from non-injured normal rats. Lung injury in the ventilated rats was confirmed by lowered blood oxygenation and reduced lung compliance as previously reported in this experimental model [30]. In addition, previous studies have also demonstrated that high V_t mechanical ventilation leads to a change in the composition of surfactant including an increase in cholesterol from 8% to 12% by weight.

Representative ToF-SIMS images of rat surfactant LB films compressed to a surface pressure of 30 mN/m are shown in Fig. 7. The palmitic acid image of the control group clearly shows the presence of domains as well as domains within domains. Saturated PLs, DPPC and DPPG, are present in domains with a higher concentration in domains within domains. The palmitic acid image of the injuriously ventilated animal group also shows the presence of domains. We have previously shown that at high enough cholesterol concentrations the percolation threshold is crossed which leads to condensed domains fusing to give large solid domains with fluid phase areas trapped within [35]. This effect can be seen in the top part of Fig. 7D which shows such a large domain as well as micron-sized condensed domains. Fig. 7E and F correspond to DPPC-H^+ and $DPPG^-$, respectively and they show that these saturated PLs are present in the micro-domains as well as the large domain "island."

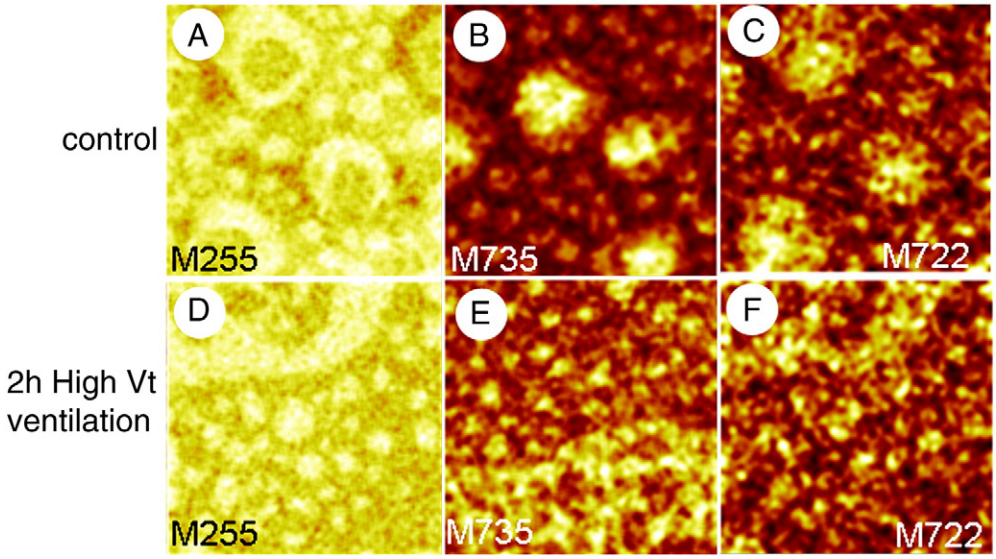

Fig. 7. ToF-SIMS images collected in positive (M735, DPPC-H^+) and negative (M255, palmitate; M722, $DPPG^-$) ion modes showing the lateral organization of LB films of pulmonary surfactant from non-injuriously ventilated (control) rats (A–C) and injuriously ventilated (2 hours high V_t ventilation) rats (D–F). Both samples were compressed to a surface pressure of 30 mN/m and transferred onto gold-coated mica by conventional Langmuir–Blodgett transfer. Images are 50×50 μm^2, 256×256 pixels and 1 shot/pixel.

4. Discussion

The objective of this paper was to present a wide range of experiments to illustrate the applicability of ToF-SIMS for surfactant research. Our results showed that ToF-SIMS could be utilized to investigate the lateral organization of surfactant interfacial films to gain information about phase separation and location of various components. By utilizing reconstituted lipid samples using deuterated analogues, we demonstrated unambiguous localization of specific lipids. Exogenous surfactant was used as a more complex model system to illustrate features of natural surfactant and the influence of added components on the lateral organization of specific components such as SP-B and cholesterol. Finally, we demonstrated that ToF-SIMS could provide lateral information on endogenous surfactant samples obtained from two different physiological conditions. Overall, these results support the concept of ToF-SIMS as a novel tool to enhance surfactant research and help elucidate, for example, the role of individual components in promoting lipid–lipid and lipid–protein interactions within the surface film and how these interactions are affected by surfactant inhibition. Such information could prove useful in furthering our understanding of surfactant function.

In order to fully comprehend the value of ToF-SIMS in surfactant research, it is important to also understand the limitations of this technique. As described in the Results, one of the limitations is the chemical similarities between different PL molecules leading to identical fragments from different molecules. In some experiments, such as those with lipid mixtures and exogenous surfactant preparation, this limitation can be resolved by including deuterium labeled analogues. We are aware that the addition of small amounts of deuterated components could perturb the phase equilibrium of a mixture, particularly when probing for minor components such as DPPG. In experiments in which the addition of deuterium analogues could impact the properties of the surfactant itself, such as endogenous surfactant from different physiological conditions, principal component analysis (PCA) of ToF-SIMS data could be performed to determine common localization of different components [32]. Another limitation of ToF-SIMS that should be considered when utilizing this technique is that the ionization/localization of specific fragments is only semi-quantitative and matrix effects have to be taken into consideration. Thus, although the fragments will define the presence of that molecule in a specific position in the surface film, the intensity of the signal is only partly related to the concentration of the molecule; other factors may influence the signal intensity such as the phase that the molecule is in and the ionization properties of the molecule. Despite these limitations, the ability of ToF-SIMS to provide a chemical compositional map of a surfactant film could be a major asset in comparing surfactant film component organization, for example with functional and dysfunctional PS. Currently, the major established techniques utilized in this area of study are atomic force microscopy, captive bubble surfactometry, fluorescence microscopy and a variety of other techniques. ToF-SIMS used in combination with these established approaches can add important additional information on surfactant properties.

Whereas our overall goal was to provide examples of specific experimental approaches to demonstrate the potential of the imaging abilities of ToF-SIMS, some of the individual experiments provided interesting results that warrant further discussion in the context of the current surfactant literature. For example, an interesting finding was the increased concentration of POPG around the edge of LC domains observed in BLES samples spiked with deuterium-labeled POPG. The implication of this finding is currently unknown but has been suggested that the net positive charge of SP-B promotes electrostatic interactions with the anionic PL fraction of surfactant, such as PG [33,36–38]. Surface tension measurements with model surfactant samples support a strong functional role for SP-B working in conjunction with anionic PL. Our finding of an increased concentration of POPG around the edge of condensed domains may be due to such interaction between POPG and SP-B. It should be noted, however, that we did not detect a similar increased concentration of miniB around the condensed domains; the low SI yield of ions specific for miniB may have limited the detection of areas of higher concentrations within the LE phase. Further studies utilizing ToF-SIMS are required and may provide direct evidence for the interaction of SP-B with POPG or other anionic PL.

A second set of specific findings worthy of further discussion relate to experiments in which cholesterol levels were altered. Considerable research has been devoted toward understanding the role of cholesterol in PS [35,39,40]. Since endogenous levels of about 5%–10% appear to be present in most mammalian surfactants, it has been suggested that this neutral lipid is important for function. Cholesterol may assist in adsorption/reinsertion of lipids to the air–liquid interface although this should be investigated further. Stronger evidence exists for the notion that elevated cholesterol leads to surfactant dysfunction. For example, adding supraphysiological amounts of cholesterol to exogenous surfactant preparations inhibits surfactant function [35,41–43] and lateral organization [35,44,45].

With respect to physiological levels of cholesterol, we utilized ToF-SIMS to make two observations. First, we showed that physiological amount of cholesterol in BLES did not affect the location of PLs or miniB, a peptide with similar surface activity as SP-B. More specifically, we show that saturated PLs remain concentrated in LC domains while unsaturated PLs and miniB are almost exclusively detected in the fluid, LE phase. These findings are in agreement with studies, utilizing a variety of other techniques, which have reported that SP-B distributes preferentially in disordered regions of membranes [39] and interfacial films [38]. Second, we observed that addition of physiological amounts of cholesterol to BLES leads to a heterogeneous distribution of DPPG within condensed domains. We have previously reported that the presence of physiological amount of cholesterol in BLES induces the formation of a new phase, Lo, within condensed domains, as determined by AFM [35]. Based on the ToF-SIMS results, it is possible to speculate that cholesterol interacts with DPPC such that segregation occurs within the solid domains where DPPC and DPPG are no longer miscible leading to regions highly concentrated in DPPG. Our data that cholesterol, when added at high physiological levels to our 3 PL mixture, was detected within condensed domains provide further support for this possible interaction with DPPC.

Effect of elevated cholesterol has been observed in the experiments using normal and injured animals. Compositional studies show a significant increase in the amount of cholesterol found in the PS of these injuriously ventilated rats compared to control. Although this increase in the level of cholesterol is believed to be a main culprit in surfactant dysfunction, we cannot exclude other compositional alterations being responsible for the observed effects. Nevertheless, we showed that the injured, high cholesterol, sample had large solid domains with fluid phase trapped within. It is likely that due to high cholesterol the percolation threshold is crossed causing LC domains to fuse. This is in agreement with our previous AFM studies of supraphysiological levels of cholesterol in BLES [35]; however, further experiments are required to provide more evidence for this speculation.

In conclusion, we show that we can successfully determine the lateral organization of surfactant interfacial films using systems varying in complexity, from PL mixtures to endogenous surfactant to natural surfactant. We show that we can detect phase separation and determine the location of PLs, cholesterol and miniB. This enables us to better understand lipid–lipid interactions, such as DPPC and cholesterol, and lipid–protein interactions, such as POPG and SP-B. Also, by studying systems with physiological levels of cholesterol, we can understand the role it plays in modulating the structure of surfactant films. Studying surfactant systems with supraphysiological levels of cholesterol, such as surfactant from injuriously ventilated rats, provides information regarding the role that cholesterol plays in surfactant dysfunction. These types of ToF-SIMS experiments

complement very well other methodologies used in surfactant research, such as AFM, fluorescence microscopy, EM, captive bubble tensiometry and others. As more information regarding surfactant function is gathered using these complementary approaches, the insight gained should prove useful in understanding the mechanisms associated with surfactant dysfunction which may lead to preparation of more effective therapeutic surfactants.

Acknowledgments

The authors would like to thank Dr. Anqiang He, ACSES, University of Alberta, for his help with ToF-SIMS imaging and Dan Vockeroth for performing the ventilation experiment. We would also like to thank BLES Biochemicals, London, Ontario for providing BLES and Dr. Robert H. Notter for his involvement with the miniB synthesis. This work was supported by the Canadian Institute of Health Research Operating Grant MOP64406. AJW, FJW and RHN were supported in this work by NIH grants HL-092158, ES-015330, HL-080775, and HL-094641.

References

[1] R. Veldhuizen, K. Nag, S. Orgeig, F. Possmayer, The role of lipids in pulmonary surfactant, Biochim. Biophys. Acta 1408 (1998) 90–108.
[2] F. Possmayer, The role of surfactant-associated proteins, Am. Rev. Respir. Dis. 142 (1990) 749–752.
[3] J. Perez-Gil, K.M. Keough, Interfacial properties of surfactant proteins, Biochim. Biophys. Acta 1408 (1998) 203–217.
[4] S. Hawgood, K. Shiffer, Structures and properties of the surfactant-associated proteins, Annu. Rev. Physiol. 53 (1991) 375–394.
[5] H. Sano, Y. Kuroki, The lung collectins, SP-A and SP-D, modulate pulmonary innate immunity, Mol. Immunol. 42 (2010) 279–287.
[6] T.E. Weaver, J.J. Conkright, Function of surfactant proteins B and C, Annu. Rev. Physiol. 63 (2001) 555–578.
[7] J. Goerke, Pulmonary surfactant: functions and molecular composition, Biochim. Biophys. Acta 1408 (1998) 79–89.
[8] A.D. Bangham, C.J. Morley, M.C. Phillips, The physical properties of an effective lung surfactant, Biochim. Biophys. Acta 573 (1979) 552–556.
[9] S. Yu, P.G. Harding, N. Smith, F. Possmayer, Bovine pulmonary surfactant: chemical composition and physical properties, Lipids 18 (1983) 522–529.
[10] R.H. Notter, Lung Surfactants, Basic Science and Clinical Applications, Marcel Dekker, Inc, New York, 2000.
[11] L.B. Ware, M.A. Matthay, The acute respiratory distress syndrome, N. Engl. J. Med. 342 (2000) 1334–1349.
[12] J.D. Merrill, R.A. Ballard, Pulmonary surfactant for neonatal respiratory disorders, Curr. Opin. Pediatr. 15 (2003) 149–154.
[13] K.J. Bosma, J.F. Lewis, Emerging therapies for treatment of acute lung injury and acute respiratory distress syndrome, Expert Opin. Emerg. Drugs 12 (2007) 461–477.
[14] J.F. Lewis, R. Veldhuizen, The role of exogenous surfactant in the treatment of acute lung injury, Annu. Rev. Physiol. 65 (2003) 613–642.
[15] J.A. Clements, Functions of the alveolar lining, Am. Rev. Respir. Dis. 115 (1977) 67–71.
[16] J.C. Watkins, The surface properties of pure phospholipids in relation to those of lung extracts, Biochim. Biophys. Acta 152 (1968) 293–306.
[17] B. Piknova, V. Schram, S.B. Hall, Pulmonary surfactant: phase behavior and function, Curr. Opin. Struct. Biol. 12 (2002) 487–494.
[18] E.C. Smith, J.M. Crane, T.G. Laderas, S.B. Hall, Metastability of a supercompressed fluid monolayer, Biophys. J. 85 (2003) 3048–3057.
[19] J.M. Crane, G. Putz, S.B. Hall, Persistence of phase coexistence in disaturated phosphatidylcholine monolayers at high surface pressures, Biophys. J. 77 (1999) 3134–3143.
[20] J.M. Crane, S.B. Hall, Rapid compression transforms interfacial monolayers of pulmonary surfactant, Biophys. J. 80 (2001) 1863–1872.
[21] S. Schurch, F.H. Green, H. Bachofen, Formation and structure of surface films: captive bubble surfactometry, Biochim. Biophys. Acta 1408 (1998) 180–202.
[22] H. Bachofen, U. Gerber, P. Gehr, M. Amrein, S. Schurch, Structures of pulmonary surfactant films adsorbed to an air–liquid interface in vitro, Biochim. Biophys. Acta 1720 (2005) 59–72.
[23] M. Amrein, A. von Nahmen, M. Sieber, A scanning force- and fluorescence light microscopy study of the structure and function of a model pulmonary surfactant, Eur. Biophys. J. 26 (1997) 349–357.
[24] R.V. Diemel, M.M. Snel, A.J. Waring, F.J. Walther, L.M. van Golde, G. Putz, H.P. Haagsman, J.J. Batenburg, Multilayer formation upon compression of surfactant monolayers depends on protein concentration as well as lipid composition. An atomic force microscopy study, J. Biol. Chem. 277 (2002) 21179–21188.
[25] S.H. Yu, F. Possmayer, Lipid compositional analysis of pulmonary surfactant monolayers and monolayer-associated reservoirs, J. Lipid Res. 44 (2003) 621–629.
[26] S. Schurch, R. Qanbar, H. Bachofen, F. Possmayer, The surface-associated surfactant reservoir in the alveolar lining, Biol. Neonate 67 (Suppl 1) (1995) 61–76.
[27] A. Benninghoven, Chemical analysis of inorganic and organic surfaces and thin films by static time-of-flight secondary ion mass spectrometry (TOF-SIMS), Angew. Chem. Int. Ed Engl. 33 (1994) 1023–1043.
[28] E.G. Bligh, W.J. Dyer, A rapid method of total lipid extraction and purification, Can. J. Biochem. Physiol. 37 (1959) 911–917.
[29] M. Sarker, A.J. Waring, F.J. Walther, K.M. Keough, V. Booth, Structure of mini-B, a functional fragment of surfactant protein B, in detergent micelles, Biochemistry 46 (2007) 11047–11056.
[30] A.A. Maruscak, D.W. Vockeroth, B. Girardi, T. Sheikh, F. Possmayer, J.F. Lewis, R.A. Veldhuizen, Alterations to surfactant precede physiological deterioration during high tidal volume ventilation, Am. J. Physiol. Lung Cell. Mol. Physiol. 294 (2008) L974–L983.
[31] J. Malloy, L. McCaig, R. Veldhuizen, L.J. Yao, M. Joseph, J. Whitsett, J. Lewis, Alterations of the endogenous surfactant system in septic adult rats, Am. J. Respir. Crit. Care Med. 156 (1997) 617–623.
[32] M.C. Biesinger, P.Y. Paepegaey, N.S. McIntyre, R.R. Harbottle, N.O. Petersen, Principal component analysis of TOF-SIMS images of organic monolayers, Anal. Chem. 74 (2002) 5711–5716.
[33] D. Breitenstein, J.J. Batenburg, B. Hagenhoff, H.J. Galla, Lipid specificity of surfactant protein B studied by time-of-flight secondary ion mass spectrometry, Biophys. J. 91 (2006) 1347–1356.
[34] S. Lund-Katz, H.M. Laboda, L.R. McLean, M.C. Phillips, Influence of molecular packing and phospholipid type on rates of cholesterol exchange, Biochemistry 27 (1988) 3416–3423.
[35] E. Keating, L. Rahman, J. Francis, A. Petersen, F. Possmayer, R. Veldhuizen, N.O. Petersen, Effect of cholesterol on the biophysical and physiological properties of a clinical pulmonary surfactant, Biophys. J. 93 (2007) 1391–1401.
[36] J. Perez-Gil, C. Casals, D. Marsh, Interactions of hydrophobic lung surfactant proteins SP-B and SP-C with dipalmitoylphosphatidylcholine and dipalmitoylphosphatidylglycerol bilayers studied by electron spin resonance spectroscopy, Biochemistry 34 (1995) 3964–3971.
[37] M. Seifert, D. Breitenstein, U. Klenz, M.C. Meyer, H.J. Galla, Solubility versus electrostatics: what determines lipid/protein interaction in lung surfactant, Biophys. J. 93 (2007) 1192–1203.
[38] K. Nag, S.G. Taneva, J. Perez-Gil, A. Cruz, K.M. Keough, Combinations of fluorescently labeled pulmonary surfactant proteins SP-B and SP-C in phospholipid films, Biophys. J. 72 (1997) 2638–2650.
[39] D.L.S. Bernardino, J. Perez-Gil, A.C. Simonsen, L.A. Bagatolli, Cholesterol rules: direct observation of the coexistence of two fluid phases in native pulmonary surfactant membranes at physiological temperatures, J. Biol. Chem. 279 (2004) 40715–40722.
[40] L.A. Bagatolli, To see or not to see: lateral organization of biological membranes and fluorescence microscopy, Biochim. Biophys. Acta 1758 (2006) 1541–1556.
[41] L. Gunasekara, S. Schurch, W.M. Schoel, K. Nag, Z. Leonenko, M. Haufs, M. Amrein, Pulmonary surfactant function is abolished by an elevated proportion of cholesterol, Biochim. Biophys. Acta 1737 (2005) 27–35.
[42] L. Gunasekara, W.M. Schoel, S. Schurch, M.W. Amrein, A comparative study of mechanisms of surfactant inhibition, Biochim. Biophys. Acta 1778 (2008) 433–444.
[43] D. Vockeroth, L. Gunasekara, M. Amrein, F. Possmayer, J.F. Lewis, R.A. Veldhuizen, Role of cholesterol in the biophysical dysfunction of surfactant in ventilator-induced lung injury, Am. J. Physiol. Lung Cell. Mol. Physiol. 298 (2010) L117–L125.
[44] Z. Leonenko, E. Finot, V. Vassiliev, M. Amrein, Effect of cholesterol on the physical properties of pulmonary surfactant films: atomic force measurements study, Ultramicroscopy 106 (2006) 687–694.
[45] Z. Leonenko, S. Gill, S. Baoukina, L. Monticelli, J. Doehner, L. Gunasekara, F. Felderer, M. Rodenstein, L.M. Eng, M. Amrein, An elevated level of cholesterol impairs self-assembly of pulmonary surfactant into a functional film, Biophys. J. 93 (2007) 674–683.